

Simultaneous second and third harmonics generation in periodically poled lithium niobate: Coupling and competition

Junming Liu(刘峻铭), Liqiang Liu(刘励强), Lihong Hong(洪丽红), and Zhiyuan Li(李志远)
Citation: Chin. Phys. B, 2025, 34 (**8**): 084203. DOI: 10.1088/1674-1056/add24a
http://cpb.iphy.ac.cn; http://iopscience.iop.org/cpb

What follows is a list of articles you may be interested in

Heterogeneous integration of silicon nitride photonics and CVD-grown WS_2 for second harmonic generation

Xuhang Jia(贾旭航), Bangren Xu(许邦仁), Jieyi Luo(罗劼舣), Ning Liu(刘宁), Yuhang Wang(王宇航), Biyuan Zheng(郑弼元), Wei Xu(徐威), and Ken Liu(刘肯)
Chin. Phys. B, 2025, 34 (**7**): 074205. DOI: 10.1088/1674-1056/adc7f7

A global model of intensity autocorrelation to determine laser pulse duration

Yufei Peng(彭雨菲), Liqiang Liu(刘励强), Lihong Hong(洪丽红), and Zhiyuan Li(李志远)
Chin. Phys. B, 2024, 33 (**5**): 054207. DOI: 10.1088/1674-1056/ad1c57

Phase-matched second-harmonic generation in hybrid polymer-LN waveguides

Zijie Wang(王梓杰), Bodong Liu(刘伯东), Chunhua Wang(王春华), and Huakang Yu(虞华康)
Chin. Phys. B, 2022, 31 (**10**): 104208. DOI: 10.1088/1674-1056/ac6edc

Second harmonic generation from precise diamond blade diced ridge waveguides

Hui Xu(徐慧), Ziqi Li(李子琦), Chi Pang(逄驰), Rang Li(李让), Genglin Li(李庚霖), Sh. Akhmadaliev, Shengqiang Zhou(周生强), Qingming Lu(路庆明), Yuechen Jia(贾曰辰), and Feng Chen(陈峰)
Chin. Phys. B, 2022, 31 (**9**): 094209. DOI: 10.1088/1674-1056/ac5242

Broadband and efficient second harmonic generation in $LiNbO_3$-$LiTaO_3$ composite ridge waveguides at telecom-band

Xin-Tong Zhang(张欣桐)
Chin. Phys. B, 2021, 30 (**1**): 014205. DOI: 10.1088/1674-1056/abb232

Simultaneous second and third harmonics generation in periodically poled lithium niobate: Coupling and competition

Junming Liu(刘峻铭)[1,2,4], Liqiang Liu(刘励强)[1,2], Lihong Hong(洪丽红)[3,2,†], and Zhiyuan Li(李志远)[1]

[1] *School of Physics and Optoelectronics, South China University of Technology, Guangzhou* 510640, *China*
[2] *Guangdong Jingqi Laser Technology Corporation Limited, Songshanhu, Dongguan* 523808, *China*
[3] *State Key Laboratory of Ultra-intense Laser Science and Technology, Shanghai Institute of Optics and Fine Mechanics, Chinese Academy of Sciences, Shanghai* 201800, *China*
[4] *School of Integrated Circuits, South China University of Technology, Guangzhou* 510640, *China*

(Received 31 March 2025; revised manuscript received 27 April 2025; accepted manuscript online 30 April 2025)

Conventional approaches for obtaining the second and third harmonics typically employ several nonlinear crystals to generate them, which is restricted in application due to the complexity of the optical path and the bulkiness of the device. In this work, we present a comprehensive theoretical and numerical investigation of the simultaneous generation and competition between the second harmonic waves (SHW) and the third harmonic waves (THW) in a single nonlinear crystal. Through analyzing both small-signal and large-signal regimes, we reveal the complex coupling mechanisms between SHW and THW generation processes. Using periodically poled lithium niobate as an example, we demonstrate that the relative conversion efficiencies between SHW and THW can be freely adjusted by controlling the input fundamental wave power. This work provides new insights for designing efficient frequency converters capable of generating both SHW and THW outputs with controllable intensity ratios.

Keywords: second harmonic generation, third harmonic generation, quasi-phase matching, periodically poled lithium niobate

PACS: 42.65.–k, 42.65.Ky, 42.70.Mp

DOI: 10.1088/1674-1056/add24a **CSTR:** 32038.14.CPB.add24a

1. Introduction

With the rapid development of ultrafast pulse lasers and artificial microstructure nonlinear materials, research into nonlinear optical phenomena has become increasingly advanced.[1] This advancement has facilitated substantial progress in the second harmonic generation (SHG),[2–4] the third harmonic generation (THG),[5–7] optical parametric processes,[8–12] supercontinuum generation (SCG),[13–16] supercontinuum white laser,[17,18] and so on. Ultrafast pulse lasers provide higher peak power, which means that the nonlinear effects of the laser through the material are more intense and the conversion efficiency is improved. The complex superlattice structure design expands the laser wavelength to a wider range, solving the limitation that laser gain media can only excite fixed wavelength lasers.

Initially, researchers focused on enhancing frequency conversion efficiency through techniques such as birefringent phase matching (BPM),[19–21] and quasi-phase matching (QPM).[22–24] QPM is achieved by periodically modulating the polarization direction in materials like $LiNbO_3$,[3] $KTiOPO_4$,[5,9,11] and $LiTaO_3$.[25] More sophisticated structures have been developed, including Fibonacci quasi-periodic superlattices[26] and chirped-periodic superlattice nonlinear crystals,[27–30] enabling more versatile frequency conversion capabilities within a single superlattice. However, for simultaneous the second harmonic wave (SHW) and the third harmonic wave (THW), both SHG and sum frequency generation (SFG) phase-matching conditions must be satisfied. These present a significant challenge since the required polarization periods for SHG and SFG are fundamentally different at common laser wavelengths. While previous studies have attempted to address this by designing superlattices that accommodate both QPM periods,[26–28] the complex theoretical calculations and stringent fabrication requirements have limited comprehensive investigations into the competitive relationship between SHG and SFG processes.

In this paper, we present a systematic theoretical framework for analyzing the competition and coupling between SHG and THG processes. Based on nonlinear coupled wave equations, we derive approximate solutions for small-signal regimes and propose an innovative approach for large-signal analysis. Using periodically poled lithium niobate (PPLN) as a model system, we demonstrate the design of a crystal structure capable of simultaneously generating both SHG and THG at a specific fundamental-wave (FW) pump laser wavelength. Through detailed numerical simulations, we show that efficient second and third harmonic outputs can be achieved while maintaining precise control over their relative energy ra-

†Corresponding author. E-mail: honglihong@siom.ac.cn

© 2025 Chinese Physical Society and IOP Publishing Ltd. All rights, including for text and data mining, AI training, and similar technologies, are reserved.

tios. Our findings provide valuable insights for designing advanced frequency converters that can generate both the SHW and THW with tunable intensity ratios, opening new possibilities for practical applications in nonlinear optics.

2. Theoretical model and computations

In the conventional method for obtaining THW, usually the FW is first passed through a frequency-doubling crystal to generate SHW, and then the obtained SHW go further to interact with the FW via the SFG process through a sum-frequency crystal, as shown in Fig. 1(a). This requires the design of two structures, and the use of birefringently matched nonlinear crystals even requires excessively long optical paths with precise delay tuning, and even the design of multi-structured superlattice matching will be subject to parametric design constraints that do not allow for free tuning. If there is a structure or nonlinear medium that can satisfy the conditions of SHG and SFG at the same time, *i.e.*, using one crystal or one structure to realize triple-frequency generation, as shown in Fig. 1(b), the combination of the advantages of each of the above mentioned will give more flexibility to the inverter design. Next, we will elaborate on the feasibility of this scheme from the theoretical model. Meanwhile, we conduct experimental simulations through numerical simulations by selecting a specific wavelength and designing the polarization period of the PPLN to ensure that it concurrently satisfies the QMP conditions of SHG and SFG.

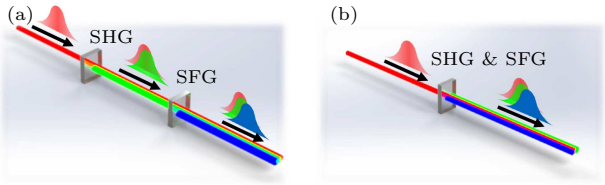


Fig. 1. Two ways to generate THW: (a) the FW passes through a frequency doubling crystal to generate SHW, and then passes through a summing crystal with FW to generate THG; (b) only one crystal is used to generate SHW and THW.

We first derive the optical field evolution of the FW during its passage through this nonlinear medium and induced nonlinear radiation. From Maxwell's equations, we obtain a general form of the time–space wave motion and evolution equation for light in a nonlinear medium:

$$\nabla^2 \boldsymbol{E} = \mu_0 \varepsilon_0 \frac{\partial^2 \boldsymbol{E}}{\partial t^2} + \mu_0 \frac{\partial^2 \boldsymbol{P}}{\partial t^2}. \tag{1}$$

Polarization $\boldsymbol{P}$ is made up of a linear and a nonlinear term:

$$\boldsymbol{P} = \boldsymbol{P}_{\mathrm{L}} + \boldsymbol{P}_{\mathrm{NL}} = \varepsilon_0 \chi \mathrm{E} + \boldsymbol{P}_{\mathrm{NL}}.$$

Here μ_0, ε_0 are vacuum permeability and vacuum permittivity, and χ is the polarizability tensor. Following standard nonlinear optics formalism, we convert the nonlinear susceptibility tensor χ to the more practical nonlinear optical coefficient d, where the relationships $\chi^{(2)}(\omega_1, \omega_2) = d(\omega_1, \omega_2)$ for SFG and $\chi^{(2)}(\omega, \omega) = 2d(\omega, \omega)$ for SHG are employed.[31]

Assuming that the incident light propagates in the positive direction along the z-axis and passes through a crystal that satisfies both SHG and SFG, we employ the slowly varying envelope approximation with paraxial wave propagation to reduce the vector wave equations to scalar coupled-mode equations. Under these conditions, the complex amplitudes of the electric field of FW, SHW, THW are $E_1(z)$, $E_2(z)$, $E_3(z)$, respectively:

$$\begin{aligned}
\frac{\mathrm{d}E_1}{\mathrm{d}z} &= \frac{\mathrm{i}\omega_1^2}{k_1 c^2}\left(d_{\mathrm{SHG}} E_2 E_1^* \mathrm{e}^{-\mathrm{i}\Delta k_{\mathrm{SHG}} z} + d_{\mathrm{SFG}} E_3 E_2^* \mathrm{e}^{-\mathrm{i}\Delta k_{\mathrm{SFG}} z}\right), \\
\frac{\mathrm{d}E_2}{\mathrm{d}z} &= \frac{\mathrm{i}\omega_2^2}{k_2 c^2}\left(\frac{d_{\mathrm{SHG}}}{2} E_1 E_1 \mathrm{e}^{\mathrm{i}\Delta k_{\mathrm{SHG}} z} + d_{\mathrm{SFG}} E_3 E_1^* \mathrm{e}^{-\mathrm{i}\Delta k_{\mathrm{SFG}} z}\right), \\
\frac{\mathrm{d}E_3}{\mathrm{d}z} &= \frac{\mathrm{i}\omega_3^2}{k_3 c^2} d_{\mathrm{SFG}} E_1 E_2 \mathrm{e}^{\mathrm{i}\Delta k_{\mathrm{SFG}} z},
\end{aligned} \tag{2}$$

where $\Delta k_{\mathrm{SHG}} = k_2 - 2k_1$ and $\Delta k_{\mathrm{SFG}} = k_3 - k_2 - k_1$ are the phase mismatches of SHG and SFG respectively, c is the speed of light in vacuum, ω_j, k_j are angular frequency and wave vector ($j = 1, 2, 3$) that correspond to the FW, SHW, and THW, d_{SHG} and d_{SFG} are the effective nonlinear coefficients of the SHG and SFG processes.

2.1. Small-signal approximations

When the conversion efficiency is not high, either due to big amount of phase mismatch or due to thin crystal length at phase matching, these equations can be solved using a small signal approximation. This approach allows us to investigate the fundamental mechanisms governing the competition between SHG and THG processes.

Starting with an initial FW of amplitude $E_1(0) = A$, and assuming negligible feedback from the generated harmonics, the evolution equations for the SHW and THW can be expressed as

$$\begin{aligned}
&E_1 = A, \\
&\frac{\mathrm{d}E_2}{\mathrm{d}z} = \frac{\mathrm{i}\omega_2^2}{k_2 c^2}\left(\frac{d_{\mathrm{SHG}}}{2} A^2 \mathrm{e}^{\mathrm{i}\Delta k_{\mathrm{SHG}} z} + d_{\mathrm{SFG}} E_3 A \mathrm{e}^{-\mathrm{i}\Delta k_{\mathrm{SFG}} z}\right), \\
&\frac{\mathrm{d}E_3}{\mathrm{d}z} = \frac{\mathrm{i}\omega_3^2}{k_3 c^2} d_{\mathrm{SFG}} A E_2 \mathrm{e}^{\mathrm{i}\Delta k_{\mathrm{SFG}} z}.
\end{aligned} \tag{3}$$

To solve this system of equations, we eliminate the variables in it and the following two equations in Eq. (3) can be written in the form of $E_3 = f_1(E_2)$, $\mathrm{d}E_3/\mathrm{d}z = f_2(E_2)$ respectively. Then, we expand $\mathrm{d}^2E_2/\mathrm{d}z^2$ by replacing the component corresponding to the inclusion of E_3, $\mathrm{d}E_3/\mathrm{d}z$. After organizing, we derive a second-order non-homogeneous linear differential equation

$$\frac{\mathrm{d}^2 E_2}{\mathrm{d}z^2} + p\frac{\mathrm{d}E_2}{\mathrm{d}z} + qE_2 = f(z),$$

where p, q are constants. Now it is possible to derive the analytic solutions of E_2, E_3. Eventually, the analytical solutions for the field amplitudes under small-signal approximation are

$$\begin{aligned}
E_1 &= A,\\
E_2 &= t\cdot\exp\left(\frac{-\mathrm{i}\Delta k_{\mathrm{SFG}}+g}{2}z\right)\\
&\quad+\left(\mathrm{i}a_1\left(\Delta k_{\mathrm{SHG}}+\Delta k_{\mathrm{SFG}}\right)r-t\right)\\
&\quad\times\exp\left(\frac{-\mathrm{i}\Delta k_{\mathrm{SFG}}-g}{2}z\right)\\
&\quad-\mathrm{i}a_1\left(\Delta k_{\mathrm{SHG}}+\Delta k_{\mathrm{SFG}}\right)r\cdot\exp\left(\frac{\mathrm{i}\Delta k_{\mathrm{SHG}}}{2}z\right),\\
E_3 &= \frac{2a_3t}{\mathrm{i}\Delta k_{\mathrm{SFG}}+g}\cdot\exp\left(\frac{\mathrm{i}\Delta k_{\mathrm{SFG}}+g}{2}z\right)\\
&\quad+\frac{2a_2\left(\mathrm{i}a_0\left(\Delta k_{\mathrm{SHG}}+\Delta k_{\mathrm{SFG}}\right)r-t\right)}{\mathrm{i}\Delta k_{\mathrm{SFG}}+g}\\
&\quad\times\exp\left(\frac{\mathrm{i}\Delta k_{\mathrm{SFG}}-g}{2}z\right)\\
&\quad-a_0a_2r\cdot\exp\left(\mathrm{i}\left(\Delta k_{\mathrm{SHG}}+\Delta k_{\mathrm{SFG}}\right)z\right),
\end{aligned}\tag{4}$$

where the coefficients are given by

$$\begin{aligned}
&a_1=\frac{\mathrm{i}\omega_2^2}{2k_2c^2}d_{\mathrm{SHG}}A^2,\quad a_2=\frac{\mathrm{i}\omega_2^2}{k_2c^2}d_{\mathrm{SFG}}A^*,\\
&a_3=\frac{\mathrm{i}\omega_3^2}{k_3c^2}d_{\mathrm{SFG}}A,\\
&g=\sqrt{-\Delta k_{\mathrm{SFG}}^2+4a_2a_3},\\
&r=\frac{1}{\Delta k_{\mathrm{SFG}}^2+\Delta k_{\mathrm{SHG}}\Delta k_{\mathrm{SFG}}+a_2a_3},\\
&t=\frac{2a_1a_2a_3\left(\Delta k_{\mathrm{SHG}}+\Delta k_{\mathrm{SFG}}\right)r}{g\Delta k_{\mathrm{SFG}}+ig^2}+\frac{a_1a_2a_3r}{g}.
\end{aligned}$$

At this point, if we make both Δk_{SHG} and Δk_{SFG} equal 0, we have

$$\begin{aligned}
E_3&=\frac{\mathrm{i}\sqrt{k_{2\omega}k_{3\omega}}}{3k_{2\omega}}\frac{d_{\mathrm{SHG}}}{d_{\mathrm{SFG}}}A\sin\left(\frac{\omega_2\omega_3}{\sqrt{k_{2\omega}k_{3\omega}}c^2}d_{\mathrm{SFG}}A\cdot z\right),\\
E_2&=\frac{1}{2}\frac{d_{\mathrm{SHG}}}{d_{\mathrm{SFG}}}A\left(\cos\left(\frac{\omega_2\omega_3}{\sqrt{k_{2\omega}k_{3\omega}c^2}}d_{\mathrm{SFG}}A\cdot z\right)-1\right).
\end{aligned}\tag{5}$$

These solutions reveal several key physical mechanisms controlling the competition between SHG and THG. The first is the phase mismatch effects, the competition dynamics are primarily governed by two phase mismatch parameters: Δk_{SHG} for SHG and Δk_{SFG} for SFG. When both Δk_{SHG} and Δk_{SFG} are non-zero, the conversion processes exhibit distinct oscillation frequencies determined by these phase mismatches. From the analytical solutions, the SHW exhibits oscillatory behavior with contributions from both phase mismatch parameters; however, under typical operating conditions where THW generation remains relatively weak, the oscillation characteristics of SHW are predominantly governed by Δk_{SHG}, as the cross-coupling terms involving Δk_{SFG} have comparatively smaller influence. Meanwhile, the THW shows a more complex modulation pattern influenced by both Δk_{SHG} and Δk_{SFG}. The second is the nonlinear coupling strengths. The effective nonlinear coefficients d_{SHG} and d_{SFG} play crucial roles in determining the relative conversion efficiencies. The ratio $d_{\mathrm{SHG}}/d_{\mathrm{SFG}}$ directly influences the competition between SHG and SFG processes. The coupling between these processes is manifested through the cross-terms in the solutions. The third is the interaction length dependencies. The crystal length z affects the conversion processes differently due to the phase mismatch terms. For phase match conditions ($\Delta k_{\mathrm{SHG}}=0$ or $\Delta k_{\mathrm{SFG}}=0$), the corresponding harmonic generation shows monotonic growth with z, while phase-mismatched processes exhibit periodic oscillations.

To illustrate these competitive effects, we examine three characteristic scenarios using a lithium niobate crystal with a 1064 nm FW:

(i) General phase mismatch situations ($\Delta k_{\mathrm{SHG}}\neq 0$, $\Delta k_{\mathrm{SFG}}\neq 0$). Here the SHW exhibits periodic oscillations primarily determined by Δk_{SHG}, while the THW shows significantly lower conversion efficiency with a complex modulation pattern influenced by both phase mismatches. The THW evolution appears as a modulated signal with its oscillation period affected by the SHG process, demonstrating the coupling between the two conversion processes, as shown in Fig. 2(a).

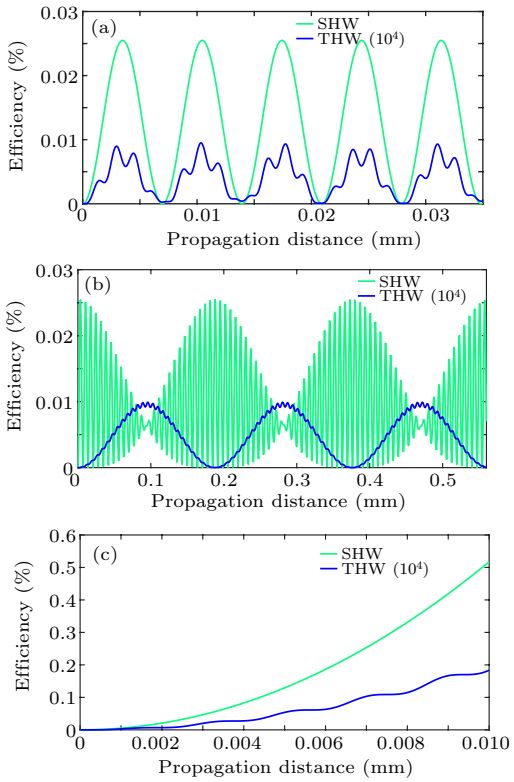


Fig. 2. Conversion efficiency evolution of 1064-nm FW through lithium niobate for SHW and THW under small signal (phase mismatch) conditions (a) the conventional case, *i.e.*, $\Delta k_{\mathrm{SHG}}\neq 0$, $\Delta k_{\mathrm{SFG}}\neq 0$; (b) $\Delta k_{\mathrm{SHG}}\neq 0$, $\Delta k_{\mathrm{SFG}}=0$; (c) $\Delta k_{\mathrm{SHG}}=0$, $\Delta k_{\mathrm{SFG}}\neq 0$; In panels (a) and (c), THW is amplified by a factor of 10^4 because the energy is too small.

(ii) $\Delta k_{\mathrm{SFG}}=0$, while Δk_{SHG} remains non-zero. In this

situation, while the SHW maintains its oscillatory behavior, the THW shows continuous energy accumulation due to phase matching. This accumulation, in turn, influences the SHG process, causing the SHW to exhibit modulation over longer propagation distances, as shown in Fig. 2(b). This scenario clearly demonstrates how phase-matched SFG can affect the SHG process through nonlinear coupling.

(iii) $\Delta k_{\mathrm{SHG}} = 0$, while Δk_{SFG} remains non-zero. In this situation, the system displays dominant SHW generation with continuous energy transfer from the fundamental wave. As shown in Fig. 2(c), the THW generation remains relatively weak but shows enhanced conversion efficiency when sufficient SHW energy is available.

In the case of the small-signal approximation, the competition mechanism can be understood through the interplay between the oscillation periods introduced by Δk_{SHG} and Δk_{SFG} terms. When both processes are phase-mismatched, the harmonic waves experience modulation by both oscillation periods, with the SHW predominantly affected by Δk_{SHG} due to the relatively low THW energy. Under phase-matched conditions for either process, the competition dynamics shift significantly, leading to either continuous energy accumulation or complex modulation patterns depending on which process is phase-matched. These analytical insights provide a fundamental understanding of the competition mechanisms in the small-signal regime, forming the basis for optimizing the relative conversion efficiencies through careful control of phase-matching conditions and nonlinear coupling strengths.

2.2. Large-signal scenarios

When both SHG and SFG processes achieve phase-matching conditions ($\Delta k_{\mathrm{SHG}} = \Delta k_{\mathrm{SFG}} = 0$) while maintain high conversion efficiency, the system enters a distinct large-signal regime characterized by complex nonlinear wave coupling. Under these conditions, the fundamental wave energy undergoes significant changes, necessitating a modified theoretical framework that accounts for energy depletion effects. The coupled-wave equations can be reformulated as

$$\begin{aligned}
\frac{\mathrm{d}E_1}{\mathrm{d}z} &= \frac{\mathrm{i}\omega_1^2}{k_1 c^2}\left(d_{\mathrm{SHG}} E_2 E_1^* + d_{\mathrm{SFG}} E_3 E_2^*\right),\\
\frac{\mathrm{d}E_2}{\mathrm{d}z} &= \frac{\mathrm{i}\omega_2^2}{k_2 c^2}\left(\frac{d_{\mathrm{SHG}}}{2} E_1 E_1 + d_{\mathrm{SFG}} E_3 E_1^*\right),\\
\frac{\mathrm{d}E_3}{\mathrm{d}z} &= \frac{\mathrm{i}\omega_3^2}{k_3 c^2} d_{\mathrm{SFG}} E_1 E_2.
\end{aligned} \tag{6}$$

If we make $\kappa = \omega_1^2/k_1 c^2 = \omega_2^2/2k_2 c^2 = \omega_3^2/3k_3 c^2$, and set $E_1(0) = 1$ to normalize the energy, then we can get

$$\begin{aligned}
E_1^2 &= \frac{1}{2}\left(1 - E_3^2\right) + \frac{1}{2}\sqrt{\left(1 - E_3^2\right)^2 + \frac{4}{9\kappa^2 d_{\mathrm{SFG}}^2}\left(\frac{\mathrm{d}E_3}{\mathrm{d}z}\right)^2},\\
E_2^2 &= -\frac{1}{2}\left(1 - E_3^2\right) + \frac{1}{2}\sqrt{\left(1 - E_3^2\right)^2 + \frac{4}{9\kappa^2 d_{\mathrm{SFG}}^2}\left(\frac{\mathrm{d}E_3}{\mathrm{d}z}\right)^2},
\end{aligned} \tag{7}$$

and E_3 can be obtained from the following differential equation:

$$\begin{aligned}
\frac{\mathrm{d}^2 E_3}{\mathrm{d}z^2} = &-\frac{3\sqrt{2}}{2}\kappa^2 d_{\mathrm{SHG}} d_{\mathrm{SFG}} \sqrt{(1 - E_3^2)^2 + \frac{4}{9\kappa^2 d_{\mathrm{SFG}}^2}\left(\frac{\mathrm{d}E_3}{\mathrm{d}z}\right)^2}\left(\left(1 - E_3^2\right) + \sqrt{(1 - E_3^2)^2 + \frac{4}{9\kappa^2 d_{\mathrm{SFG}}^2}\left(\frac{\mathrm{d}E_3}{\mathrm{d}z}\right)^2}\right)^{1/2}\\
&-3\kappa^2 d_{\mathrm{SFG}}^2 E_3\left(\frac{3}{2}(1 - E_3^2) + \frac{1}{2}\sqrt{(1 - E_3^2)^2 + \frac{4}{9\kappa^2 d_{\mathrm{SFG}}^2}\left(\frac{\mathrm{d}E_3}{\mathrm{d}z}\right)^2}\right).
\end{aligned} \tag{8}$$

Equation (8) demonstrates that THW generation is influenced by the coupled SHG–SFG process. The first term represents the combined effect of SHG and SFG, while the second term solely depends on SFG. The ratio between these terms is approximately $d_{\mathrm{SHG}}/d_{\mathrm{SFG}}$, indicating that the competition becomes more pronounced when the effective nonlinear coefficients are comparable.

To better illustrate these complex dynamics, we use a normalized coordinate system space, which normalizes the physical quantities ($\kappa = 1$, $d_{\mathrm{SHG}} = 1$, $d_{\mathrm{SFG}} = \eta d_{\mathrm{SHG}}$, $n_1 = 1$), and rewrite Eq. (6) as

$$\begin{aligned}
\frac{\mathrm{d}E_1}{\mathrm{d}z} &= \mathrm{i}\left(E_2 E_1^* + \eta E_3 E_2^*\right),\\
\frac{\mathrm{d}E_2}{\mathrm{d}z} &= \mathrm{i}\left(E_1 E_1 + 2\eta E_3 E_1^*\right),\\
\frac{\mathrm{d}E_3}{\mathrm{d}z} &= \mathrm{i}3\eta E_1 E_2.
\end{aligned} \tag{9}$$

Our numerical analysis upon Eq. (9), implemented using the fourth-order Runge–Kutta method,[32,33] reveals rich dynamical behavior in the large-signal regime. Through theoretical analysis, we further reveal that the phase relationships between the three waves play a crucial role in determining the energy flow directions. When the FW amplitude is positive and real, the SHW field exhibits a purely imaginary nature, while the THW field maintains a negative real value. These phase relationships correspond to the electric field polarization states of the three waves and directly influence their coupling

dynamics.

Figures 3(a) and 3(b) illustrate the evolution of the relative energies and amplitudes of the three waves, demonstrating complex periodic oscillations. To better understand these dynamics, we assume that this period is Ω and transform the transverse coordinates z to $\sin(\Omega z)$ or $\cos(\Omega z)$. As shown in Figs. 3(c)–3(e), they reveal three distinct periodic components in the system's evolution. These components follow oval-shaped trajectories, suggesting that the coupled competing solutions of SHG and SFG obey an ovoid function with three cycles, corresponding to the three-wave evolution conforming Jacobi elliptic function in regular SFG processes.

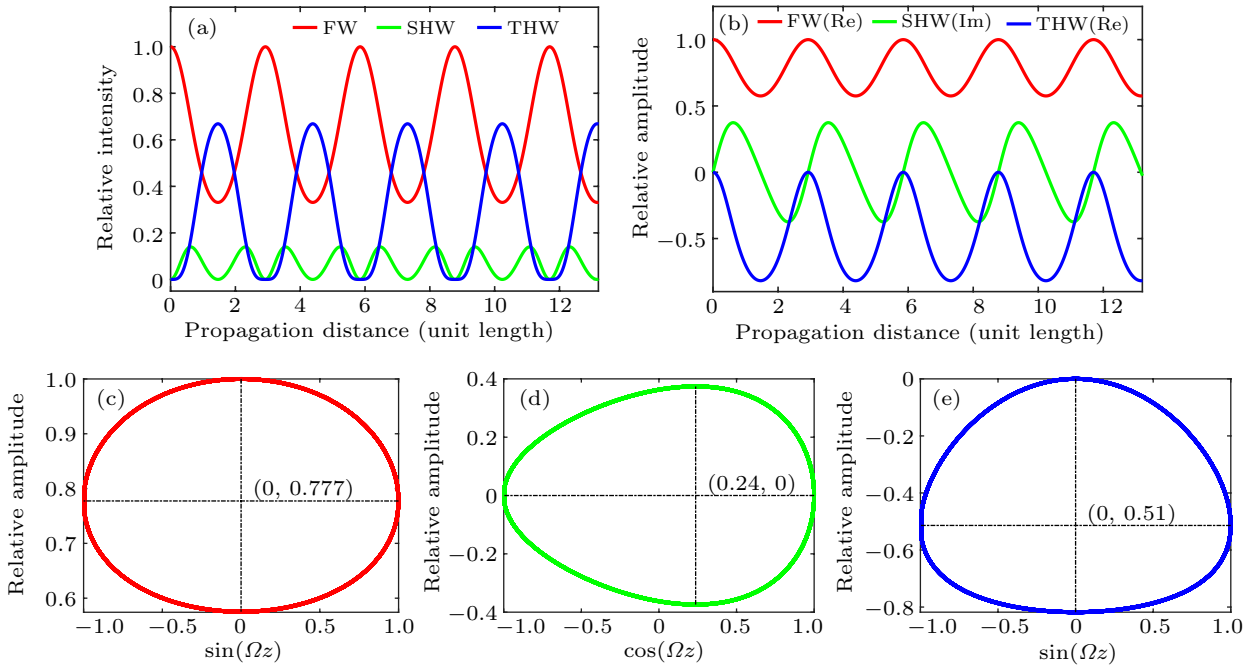


Fig. 3. The FW passes through a single crystal to generate both SHW and THW in the case of large signals: (a) evolution of energy conversion efficiency for three waves, (b) amplitude evolution of three waves, (c)–(e) oscillatory map based on the amplitude period of FW, SHW, and THW.

The system behavior is primarily controlled by the ratio $d_{\mathrm{SHG}}/d_{\mathrm{SFG}}$. When this ratio is significantly small ($d_{\mathrm{SHG}}/d_{\mathrm{SFG}} \ll 1$), the system demonstrates suppressed THW generation due to the dominant SHG process. In this regime, the SHW remains in a low-energy state because its generation rate is substantially lower than its consumption rate through the SFG process. Consequently, the system behavior closely approximates the small-signal regime described by our earlier analytical solutions (Eq. (5)), exhibiting quasi-sinusoidal oscillations with a single dominant period.

Conversely, when $d_{\mathrm{SHG}}/d_{\mathrm{SFG}} \gg 1$, rapid FW depletion occurs, leading to insufficient energy for sustained THW generation. This scenario results in predominant conversion to SHW, despite initial THW production. A characteristic example of this behavior is illustrated in Fig. 4(a), where the THW generation exhibits an initial growth phase followed by energy reversal as the fundamental wave becomes depleted.

Most intriguingly, we discover a critical ratio ($d_{\mathrm{SHG}}/d_{\mathrm{SFG}}$) where the system undergoes a qualitative transition in its dynamics. At this critical point, which is determined by

$$\frac{d_{\mathrm{SHG}}}{d_{\mathrm{SFG}}} \approx 1.53426,$$

the system achieves optimal conditions for THW generation, resulting in complete energy transfer from both FW and SHW to THW. This critical condition represents a unique operating point where the system neither exhibits periodic oscillations nor defaults to dominant SHW production, as demonstrated in Fig. 4(b).

In conclusion to the above discussions, by manipulating the ratio of $d_{\mathrm{SHG}}/d_{\mathrm{SFG}}$, the competition dynamics between SHG and SFG can be altered. Initially, SHW exhibits the highest conversion efficiency, while THW remains at zero. During this phase, both SHG and SFG processes occur. As time proceeds, the conversion efficiency of THW gradually increases, surpassing that of SHW, leading to a decrease in the total energy of SHW. When THW reaches its first peak, at least one of FW or SHW will be depleted. If $d_{\mathrm{SHG}}/d_{\mathrm{SFG}}$ is large enough so that only the energy of FW is exhausted first, the THW and SHW will undergo the difference frequency generation (DFG) process, resulting in FW that maintains the same polarization direction as the original FW but with a phase shift of π. On the one hand, the energy of THW is derived from the DFG process, while on the other hand, the generated FW will be consumed through SHG, ultimately converting energy into SHW. Otherwise, if $d_{\mathrm{SHG}}/d_{\mathrm{SFG}}$ is small enough so that only the energy of SHW is exhausted first, THW and FW will also produce SHW with opposite phases via DFG. Subsequently,

the energy of THW will be consumed, with some producing SHW alongside with FW, while the remainder generates FW with SHW, leading to a final energy conversion to FW and initiating the next periodic evolution. If both SHW and FW are depleted simultaneously, the energy will be transformed into THW.

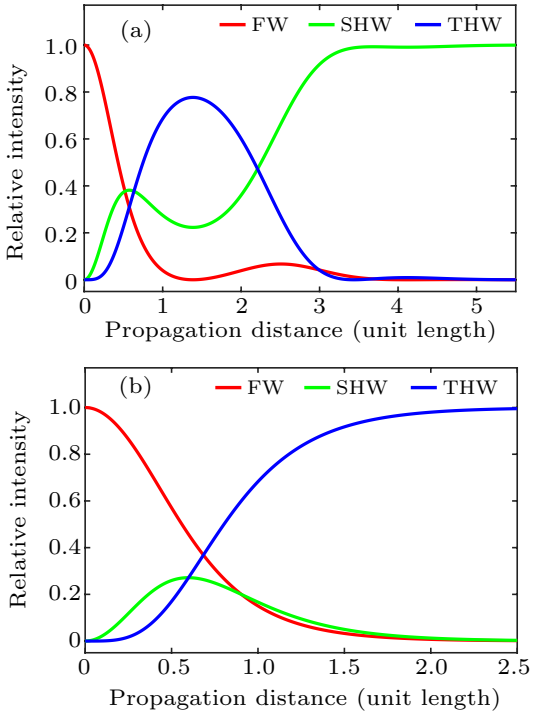


Fig. 4. Two special cases under the large-signal numerical solution: (a) $d_{\mathrm{SHG}}/d_{\mathrm{SFG}} > 1.54$, here $d_{\mathrm{SHG}}/d_{\mathrm{SFG}}$ is set to 2, (b) $d_{\mathrm{SHG}}/d_{\mathrm{SFG}} \approx 1.53426$.

This comprehensive understanding of large-signal dynamics provides crucial insights for designing efficient frequency conversion devices. The ability to control the relative conversion efficiencies through careful selection of the nonlinear coupling ratio offers new possibilities for tailoring the output spectrum for specific applications. Moreover, the identification of the critical coupling ratio establishes a clear design target for optimizing THW generation efficiency.

3. Numerical simulation

To validate our theoretical analysis and demonstrate practical applications of simultaneous SHG and THG, we conduct comprehensive numerical simulations using PPLN as a model system. The key to achieving efficient coupled wave generation lies in selecting appropriate QPM conditions that simultaneously satisfy both SHG and THG processes. We chose 5-mol% MgO:PPLN as the nonlinear medium, whose refractive index follows the Sellmeier equation[34]

$$\begin{aligned} n_{\mathrm{e}}^2 &= 5.756 + 2.860\times10^{-6} f \\ &\quad + \frac{0.0983 + 4.700\times10^{-8} f}{\lambda^2 - (0.2020 + 6.113\times10^{-8} f)^2} \\ &\quad + \frac{189.32 + 1.516\times10^{-4} f}{\lambda^2 - 12.52^2} - 1.32\times10^{-2}\lambda^2, \end{aligned} \tag{10}$$

where λ is the wavelength corresponding to the FW, and f represents the temperature-dependent term

$$\begin{aligned} f &= (T - T_0)(T + T_0 + 2\times273.16) \\ &= (T - 24.5\ ^{\circ}\mathrm{C})(T + 570.82). \end{aligned}$$

Here we set the temperature $T = 26\ ^{\circ}\mathrm{C}$. The QPM conditions for SHG and SFG can be expressed as

$$\Lambda_{\mathrm{SHG}}(m) = m\frac{2\pi}{\Delta k_{\mathrm{SHG}}}, \quad \Lambda_{\mathrm{SFG}}(m) = m\frac{2\pi}{\Delta k_{\mathrm{SFG}}}, \tag{11}$$

where Λ_{SHG} and Λ_{SFG} are the QPM periods of SHG and SFG, m is an odd multiple of the coefficient to satisfy the quasi-phase matching, and

$$\begin{aligned} \Delta k_{\mathrm{SHG}} &= k_2 - 2k_1 = \frac{4\pi}{\lambda}\left(n_{\mathrm{e}}(\lambda/2) - n_{\mathrm{e}}(\lambda)\right), \\ \Delta k_{\mathrm{SFG}} &= k_3 - k_2 - k_1 \\ &= \frac{2\pi}{\lambda}\left(3n_{\mathrm{e}}(\lambda/3) - 2n_{\mathrm{e}}(\lambda/2) - n_{\mathrm{e}}(\lambda)\right). \end{aligned}$$

These equations must satisfy the following relationship $\Lambda_{\mathrm{SHG}}(m_1) = \Lambda_{\mathrm{SHG}}(m_2)$. To obtain a high conversion efficiency, the smaller the values of m_1 and m_2, the better. For PPLN, we generally set $m_1 = 1$. Since $m_2 = 1$ has no solution, we step back and use $m_2 = 3$. Through careful analysis of the QPM periods $\Lambda_{\mathrm{SHG}}(m = 1)$ and $\Lambda_{\mathrm{SFG}}(m = 3)$ as functions of the fundamental wavelength (Fig. 5), we identify an optimal operating point at $\lambda = 1.4089$ μm. This wavelength selection ensures that the QPM periods for SHG and SFG are closely matched, with symmetric positive and negative domain structures (50% duty cycle) and polarization period length $\Lambda = 15.459$ μm providing QPM for SFG while maintaining controlled phase mismatch for SHG to regulate the competition between the two processes.

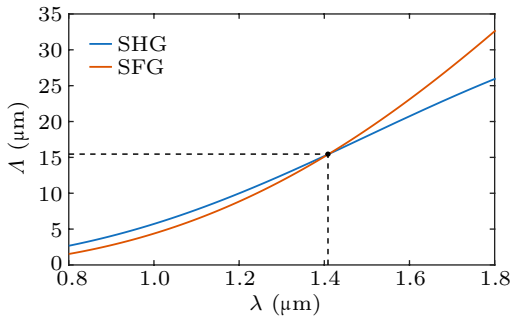


Fig. 5. Polarization period $\Lambda_{\mathrm{SHG}}(m = 1)$ and $\Lambda_{\mathrm{SFG}}(m = 3)$ of PPLN corresponding to SHG and SFG for different wavelength QPM cases.

For accurate analyze the nonlinear interactions, we represent the effective nonlinear coefficients of QPM process through Fourier transform:

$$d(G_{\mathrm{m}}) = \frac{1}{L}\int_0^{\mathrm{L}} \mathrm{d}(z)\exp(-\mathrm{i}G_{\mathrm{m}}z)\,\mathrm{d}z, \tag{12}$$

where L is the through-light length of the entire crystal, G_{m} are the reciprocal lattice vectors (RLV), and $d(z)$ is the effective

nonlinearity coefficient at the z position, which is satisfied for each period Λ in PPLN:

$$d(z) = \begin{cases} +d_{\text{eff}}, & 0 \le z < \dfrac{\Lambda}{2}, \\ -d_{\text{eff}}, & \dfrac{\Lambda}{2} \le z < \Lambda. \end{cases}$$

Let each domain length be l_m, the effective nonlinear coefficients for SHG and SFG are calculated as

$$d_{\text{SHG}} = d_{\text{eff}} \frac{1}{L} \sum_m (-1)^m l_m \exp(-\mathrm{i}\, \mathrm{d} k_{\text{SHG}} z) \approx \frac{2}{\pi} d_{\text{eff}}, \quad (13)$$

$$d_{\text{SFG}} = d_{\text{eff}} \frac{1}{L} \sum_m (-1)^m l_m \exp(-\mathrm{i}\, \mathrm{d} k_{\text{SFG}} z) \approx \frac{2}{3\pi} d_{\text{eff}}. \quad (14)$$

We implement the fourth order Runge–Kutta method to solve the coupled wave equations numerically, with careful consideration of step size (Δz) to ensure computational accuracy. Here we assume that the electric field amplitude of the input FW pump laser is 3×10^7 V/m (corresponding to an example pulse laser with parameters as 10 ps, beam radius 0.1 mm, and single pulse energy 400 nJ).

Our numerical simulations reveal the complex dynamics in the competition between SHG and THG processes (Fig. 6). The evolution can be characterized by several distinct phases. Initially, the system closely follows theoretical predictions, with all three waves showing an evolution consistent with the above theory. The FW experiences significant depletion, reaching its minimum at $z \approx 2.6$ mm. At this point, we observe an abrupt phase shift in the FW (Fig. 6(b)), marking the onset of DFG between THW and SHW as a new source of fundamental wave energy. Subsequently, the competition enters a more complex phase characterized by benign competition between THW and SHW, phase-dependent cancellation of the FW generated by the SFG and consumed by the SHG, and continuous energy exchange through cascaded nonlinear processes. This continues until the SHW energy reaches depletion at $z \approx 8.6$ mm. At this point, accompanied by a π phase shift (Fig. 6(c)), initiating a new mode of DFG between the THW and FW. After that, SHW and THW alternatively achieve higher conversion efficiencies, though with increasing complexity due to accumulated phase mismatch.

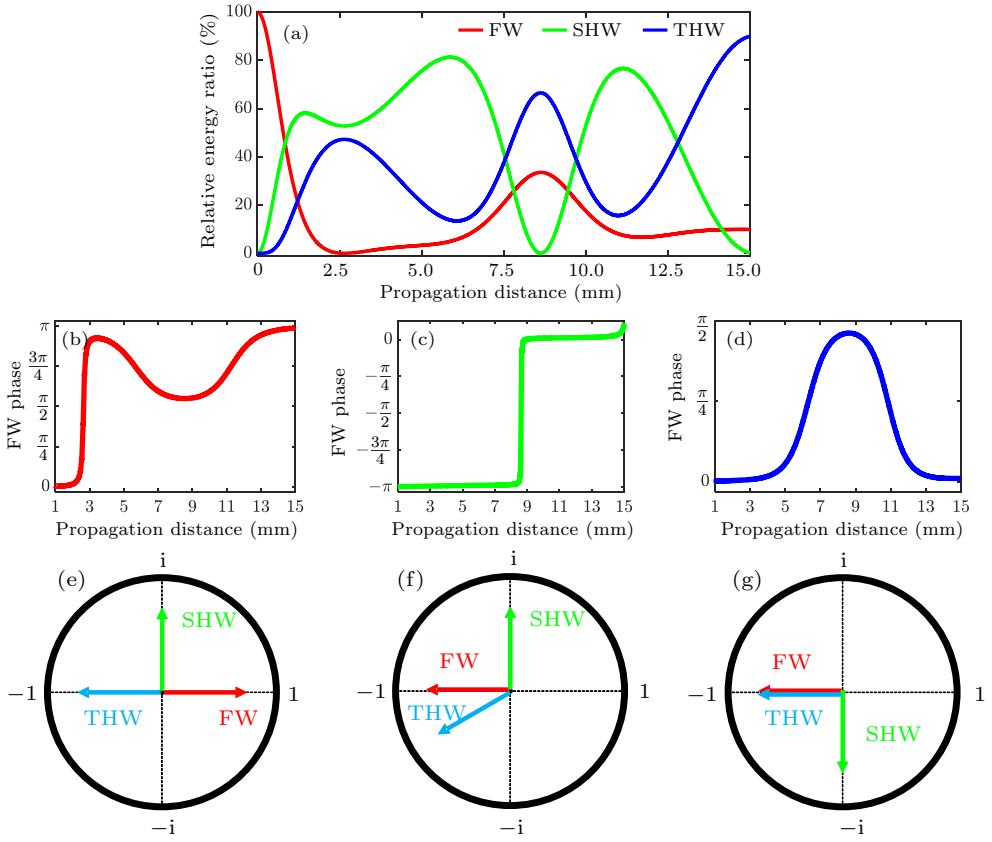


Fig. 6. Numerical simulation of 1.4089 μm FW by the design of PPLN for three waves (a) evolutionary diagram of the energy of the three waves, (b) phase evolution diagram of FW, (c) phase evolution diagram of SHW, (d) phase evolution diagram of THW, (e)–(g) schematic diagram of the phases of the three waves in the complex plane at $1 \le z \le 2.6$, $2.6 < z \le 8.6$, $8.6 < z \le 15$.

One of the most significant findings from our simulations is the ability to control the relative conversion efficiencies through input power modulation (Fig. 7). It illustrates a remarkable control capability, showing the final conversion efficiencies of all three waves as a function of input FW energy. The clear periodic structure in the efficiency curves underscores the deterministic nature of the power-dependent control mechanism, providing a robust framework for designing application-specific frequency converters.

By systematically varying the input field amplitude, we

demonstrate precise manipulation of energy distribution between SHG and THG processes. When the input electric field amplitude $E_1(0)$ is approximately 1.93×10^7 V/m or 3.11×10^7 V/m, the system exhibits preferential conversion to THW with near-complete depletion of SHW, effectively achieving direct THG. Conversely, at input amplitudes around 1.34×10^7 V/m and 2.40×10^7 V/m, the process strongly favors SHW generation, maintaining minimal energy levels in both FW and THW components. Most intriguingly, at intermediate field strengths such as 1.73×10^7 V/m, the system achieves simultaneous high-efficiency conversion to both harmonics.

This power-dependent behavior arises from the intricate interplay between coupled nonlinear processes and phase-matching conditions. At lower input powers, the conversion dynamics are primarily governed by the initial SHG process, with subsequent SFG occurring as a secondary effect. As the input power increases, the coupled wave interactions become more complex, leading to enhanced competition between SHG and SFG processes. The observed periodic variation in conversion efficiencies with input power suggests a fundamental relationship between the input field strength and the relative strengths of competing nonlinear processes.

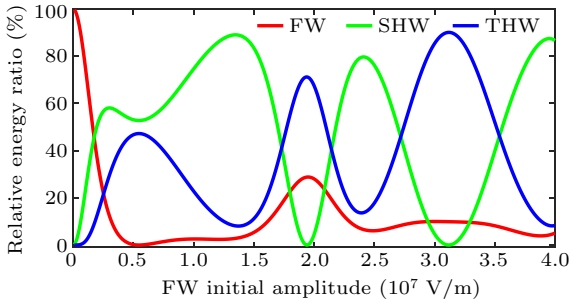


Fig. 7. Final conversion efficiency plots of three waves at different input energies of FW.

Our numerical results demonstrate the feasibility of using a single PPLN crystal for efficient and controllable multi-harmonic generation. The simulation results suggest that optimal performance requires appropriately limit on the crystal length to maintain manageable phase mismatch accumulation. The ability to tune the relative intensities of SHW and THW through input power modulation provides a wide range of application scenarios. Compared to traditional multiple-crystal arrangements, the current single PPLN crystal scheme not only simplifies the optical setup and reduces the number of required optics, but also improves system stability for compact integrated frequency conversion devices. This finding provides important guidance for practical device design and implementation. This ability to selectively control harmonic generation through simple power adjustment represents a significant advancement over traditional methods requiring physical modification of crystal structures or complex multiple-crystal arrangements.

This tunability enables unprecedented flexibility in spectral engineering, allowing for dynamic switching between single-harmonics and dual-harmonics operation modes. Furthermore, the continuous nature of this control mechanism facilitates fine-tuning of the output spectrum for specific application requirements, such as wavelength-sensitive spectroscopy or multi-color imaging systems.

4. Conclusions

In summary, we have presented a comprehensive theoretical and numerical investigation of the simultaneous generation and competition between SHW and THW in a single nonlinear crystal. Through systematic analysis of both small-signal (at phase mismatching situations) and large-signal (at phase matching situations) regimes, we have revealed several key findings. First, in the small-signal approximation, we derive analytical solutions by varying phase-matching conditions (Δk_{SHG} and Δk_{SFG}), which elucidates the fundamental competition dynamics between SHW and THW generation. Our analysis shows that when both processes are phase-mismatched, SHW and THW exhibit modulated oscillation periods, with SHW primarily affected by Δk_{SHG} due to the relatively low THW energy. When SFG achieves phase-matching, both waves become modulated by Δk_{SHG}, while phase-matched SHG results in continuous energy transfer to SHW. Second, for large-signal scenarios, we demonstrate that the competition between SHG and SFG can be controlled by adjusting the ratio of their effective nonlinear coefficients ($d_{\mathrm{SHG}}/d_{\mathrm{SFG}}$). Our numerical analysis reveals that the electric field amplitudes of the three waves evolve as a three-period oval function when phase-matched. Notably, we identify a critical ratio ($d_{\mathrm{SHG}}/d_{\mathrm{SFG}} \approx 1.53426$) at which complete energy conversion to THW becomes possible, providing a theoretical foundation for optimizing conversion efficiency. Furthermore, using MgO:PPLN as a model system, we design and numerically simulate a crystal structure capable of simultaneously generating both harmonics. Our simulations demonstrate that the energy distribution between SHW and THW can be precisely controlled by adjusting the input fundamental wave power. This finding has significant practical implications, as it enables: (i) selective generation of high-efficiency SHW or THW independently, (ii) simultaneous generation of both harmonics with tunable intensity ratios, (iii) dynamic control of the output spectrum through input power modulation.

The proposed single-crystal setup offers several advantages over conventional multiple-crystal setups, including reduced system complexity, improved stability, and enhanced flexibility in frequency converter design. Our theoretical framework and numerical results provide valuable guidelines

for developing next-generation nonlinear optical devices capable of efficient and controllable multi-harmonic generation. This work not only advances our understanding of the fundamental physics governing harmonic generation competition but also opens up new possibilities for practical applications in frequency conversion, ultrafast optics, and spectroscopy. Future work could focus on extending this approach to other nonlinear materials and exploring more complex multi-wave mixing processes.

Acknowledgements

Project supported by the Science and Technology Project of Guangdong Province, China (Grant No. 2020B010190001), the National Natural Science Foundation of China (Grant No. 12434016), the National Key Research and Development Program of China (Grant No. 2023YFA1406900), and the Fund of the National Postdoctoral Researcher Program (Grant No. GZB20240785).

References

[1] Agrawal G 2013 *Nonlinear Fiber Optics*, 5th ed. (Oxford: Elsevier)
[2] Wang G, Lu J, Cui D, Xu Z, Wu Y, Fu P, Guan X and Chen C 2002 *Opt. Commun.* **209** 481
[3] Lenhardt F, Nebel A, Knappe R, Nittmann M, Bartschke J and L'huillier J 2010 *Presented at the Conference on Lasers and Electro-Optics* 2010, (California: San Jose)
[4] Konforty N, Cohen M, Segal O, Plotnik Y and Segev M 2024 *Light: Sci. Appl.* **14** 152
[5] Mu X and Ding Y 2001 *Opt. Lett.* **26** 623
[6] Huang C and Zhu Y 2005 *Phys. Status Solidi B* **242** 1694
[7] Feve J, Boulanger B and Guillien Y 2000 *Opt. Lett.* **25** 1373
[8] Hsu C, Lai J, Hsu C, Huang Y, Wu K and Chou M 2019 *Presented at the Conference on Nonlinear Frequency Generation and Conversion - Materials and Devices XVIII, San Francisco, CA*
[9] Wang W, Cong Z, Chen X, Zhang X, Qin Z, Tang G, Li N, Wang C and Lu Q 2014 *Opt. Lett.* **39** 3706
[10] Antipov O, Kolker D, Dobrynin A, Zav'yalov A, Getmanovskiy Y, Sharkov V, Chuvakova M, Akhmathanov A and Shur V 2022 *International Conference Laser Optics (ICLO)* **1** 1
[11] Zukauskas A, Thilmann N, Pasiskevicius V, Laurell F and Canalias C 2009 *Appl. Phys. Lett.* **95** 191103
[12] Antipov O, Kolker D, Dobrynin A, Getmanovskii Y, Sharkov V, Chuvakova M, Akhmatkhanov A, Shur V, Shestakova I and Larin S 2022 *Quantum Electron.* **52** 254
[13] Feng Z, Lan J, Li W, Liu X, Yu C, Li J and Liu Y 2020 *Phys. Plasmas* **27** 023302
[14] Lu J, Surya J, Liu X, Xu Y and Tang H 2019 *Opt. Lett.* **44** 1492
[15] Yu M, Shao L, Okawachi Y, Gaeta A, and Loncar 2020 *Conference on Lasers and Electro-Optics (CLEO)* STu4H 1
[16] Genier E, Grelet S, Engelsholm R, Bowen P, Moselund P, Bang O, Dudley J, and Sylvestre T 2022 *Opt. Lett.* **47** 2064
[17] Hong L, Hu C, Liu Y, He H, Liu L, Wei Z and Li Z 2023 *PhotoniX* **4** 11
[18] Chen B, Zhang C, Hu C, Liu R and Li Z 2015 *Phys. Rev. Lett.* **115** 083902
[19] Giordmaine J 1962 *Phys. Rev. Lett.* **8** 19
[20] Maker P, Terhune R, Nisenoff M and Savage C 1962 *Phys. Rev. Lett.* **8** 21
[21] Zhang X, Wang Z, Wang G, Zhu Y, Xu Z and Chen C 2009 *Opt. Lett.* **34** 1342
[22] Armstrong J, Bloembergen N, Ducuing J and Pershan P 1962 *Phys. Rev.* **127** 1918
[23] Fejer M, Magel G, Jundt D and Byer R 1992 *IEEE J. Quantum Electron.* **28** 2631
[24] Ren M and Li Z 2011 *Europhys. Lett.* **94** 44003
[25] Demkin A, Baranov A, Ahtyamov V and Myasnikov D 2016 *Presented at the* 2016 *International Conference Laser Optics (LO)*
[26] Chen Y, Zhu Y, Qin Y, Zhang C, Zhu S and Ming N 2000 *J. Phys.: Condens. Matter* **12** 529
[27] Chen B, Ren M, Liu R, Zhang C, Sheng Y, Ma B and Li Z 2014 *Light: Sci. Appl.* **3** e189
[28] Tao Y, Zhu W, Zhang Y, Ma J, Wang J, Yuan P, Zhang H, Zhu H and Qian L 2024 *Chin. Opt. Lett.* **22** 011901
[29] Li M, Hong L and Li Z 2022 *Research* **2022** 9871729
[30] Chen B, Hong L, Hu C and Li Z 2021 *Research* **2021** 1539730
[31] Shen Y 1977 *Nonlinear Infrared Generation* (Berlin: Springer)
[32] Hu C, He H, Chen B, Wei Z and Li Z 2017 *J. Appl. Phys.* **122** 243105
[33] Hong L, Chen B, Hu C and Li Z 2021 *J. Appl. Phys.* **129** 233101
[34] Gayer O, Sacks Z, Galun E and Arie A 2008 *Appl. Phys. B* **91** 343